Journal of Innovative Optical Health Sciences
Vol. 2, No. 4 (2009) 343–352

World Scientific
www.worldscientific.com

DEVELOPMENT OF NEEDLE-BASED MICROENDOSCOPY FOR FLUORESCENCE MOLECULAR IMAGING OF BREAST TUMOR MODELS

CHAO-WEI CHEN[†], TIFFANY R. BLACKWELL[‡],
RENEE NAPHAS[†], PAUL T. WINNARD JR.[‡], VENU RAMAN[‡],
KRISTINE GLUNDE[*,‡,¶] and YU CHEN[*,†,§]
[†]*Fischell Department of Bioengineering and*
Electrical and Computer Engineering, University of Maryland
College Park, MD 20742, USA
[‡]*In Vivo Cellular and Molecular Imaging Center (ICMIC)*
Department of Radiology, Johns Hopkins University School of Medicine
Baltimore, MD 21205, USA
[§]*yuchen@umd.edu*
[¶]*kglunde@mri.jhu.edu*

Fluorescence molecular imaging enables the visualization of basic molecular processes such as gene expression, enzyme activity, and disease-specific molecular interactions *in vivo* using targeted contrast agents, and therefore, is being developed for early detection and *in situ* characterization of breast cancers. Recent advances in developing near-infrared fluorescent imaging contrast agents have enabled the specific labeling of human breast cancer cells in mouse model systems. In synergy with contrast agent development, this paper describes a needle-based fluorescence molecular imaging device that has the strong potential to be translated into clinical breast biopsy procedures. This microendoscopy probe is based on a gradient-index (GRIN) lens interfaced with a laser scanning microscope. Specifications of the imaging performance, including the field-of-view, transverse resolution, and focus tracking characteristics were calibrated. Orthotopic MDA-MB-231 breast cancer xenografts stably expressing the tdTomato red fluorescent protein (RFP) were used to detect the tumor cells in this tumor model as a proof of principle study. With further development, this technology, in conjunction with the development of clinically applicable, injectable fluorescent molecular imaging agents, promises to perform fluorescence molecular imaging of breast cancers *in vivo* for breast biopsy guidance.

Keywords: Breast cancer; fluorescence molecular imaging; microendoscopy; optical imaging; tdTomato fluorescent protein.

1. Introduction

The American Cancer Society estimates that 192,370 women will be diagnosed with breast cancer and that 40,170 women will die of breast cancer in the United States alone in 2009.[1] One in eight women born today is likely to be diagnosed with breast cancer during their lifetime. Over the past decade, positive trends are evident as a result of

*Corresponding authors.

innovations in early diagnosis and treatment. However, a substantial percentage of early cancers are still missed suggesting that detection methods still need to be improved. Conventional needle-based biopsy techniques have the disadvantage of false-negative rates as a result of sampling errors.[2,3] Image-guided biopsy is advantageous for enhancing sampling success rates.[4,5] However, improvements are limited to lesions that are visible on ultrasound or mammography. Both imaging techniques have limited resolutions and sensitivities.[6,7] Therefore image-guided biopsy using those imaging methods cannot adequately identify early lesions or localize the precise extent of lesions. In addition, the microscopic changes associated with early neoplastic pathologies are still beyond the reach of clinicians during the biopsy procedure. Therefore, there exists a critical need for development of more sensitive and specific imaging techniques that can accurately detect and characterize breast cancer *in situ* and in real time to guide biopsy procedures with the aim of improving sampling accuracy.

Over the past decade, optical methods based on light–tissue interactions (including scattering, absorption, and fluorescence) have been developed to image and diagnose early neoplastic changes in the breast. Various optical technologies including diffuse optical tomography and spectroscopy,[8–13] fluorescence and reflectance spectroscopy,[14–17] optical coherence tomography (OCT),[18–20] fluorescence molecular tomography and imaging,[21–25] and confocal and multi-photon microscopy,[26–31] have emerged as technologies with the potential for detection and characterization of breast cancer *in vivo*. Using fiber optics and micro-optics technology, optical methods can be miniaturized into needle-based imaging devices for detection of breast tumors *in vivo* and to guide needle biopsy procedures.[32–36] These optically based methods are being developed to further improve diagnostic accuracy by reducing false-negative rates, which at present are generated from sampling errors due to limitations of the present guided biopsy protocols.

Specifically, fluorescence molecular imaging enables the visualization of basic molecular processes such as gene expression, enzyme activity, and disease-specific molecular interactions *in vivo* using targeted contrast agents.[37–41] Therefore, fluorescence molecular imaging is being developed for early detection and *in situ* characterization of cancers by targeting distinct cancer cell molecular signatures.[42,43] Near-infrared fluorescent imaging contrast agents have recently been developed to improve detection of breast cancer.[22,25,44] These agents target either specific biological processes such as lysosome accumulation,[25] or biomarkers such as differentially expressed cellular proteins, or are activated by specific enzymes that are relatively specific for cancer.[22,44] In addition, near-infrared fluorescence imaging systems (including fluorescence reflectance imaging,[25,45–47] fluorescence molecular tomography,[22,48] wide-field microscopy, confocal and multi-photon microscopy) have been developed for fluorescence molecular imaging to various depths, magnifications, and resolution scales. Macroscopic fluorescence molecular tomography and reflectance imaging, although able to image deep into tissue, are limited by their imaging resolutions and are unable to visualize cellular- or subcellular-scale molecular activities. Standard microscopic technologies, although providing high resolution for *in vivo* molecular imaging, are limited by their optical penetration depth ($\sim$500 μm) and therefore cannot reach deep tissue. More invasive procedures, such as surgery, are required to expose the tissue under the microscope.

Minimally invasive procedures involving the insertion of miniature needle imaging devices represent an effective approach to imaging deep tissue with microscopy. Gradient-index (GRIN) lens or MicroProbe Objective (MPO)-based miniature focusing optics have been demonstrated as having the ability to image deep tissues with confocal, two-photon, and coherence anti-Stokes Raman scattering (CARS) microscopy.[49–53] In this paper, we report the development and characterization of a needle-based fluorescence molecular microendoscopy imaging device, which potentially has applications in the imaging of breast cancer *in vivo*.

2. Methods

2.1. *System configurations*

Figure 1(a) shows the diagram of the fluorescence microscopy imaging system. The fluorescence microscopy system used a continuous-wave (CW) laser diode as the excitation source. Different excitation wavelengths could be chosen depending on the specific fluorescence markers or contrast agents under investigation. The excitation light was focused by a microscope objective onto the needle microendoscope to illuminate the tissue. The fluorescence light was collected by the objective and

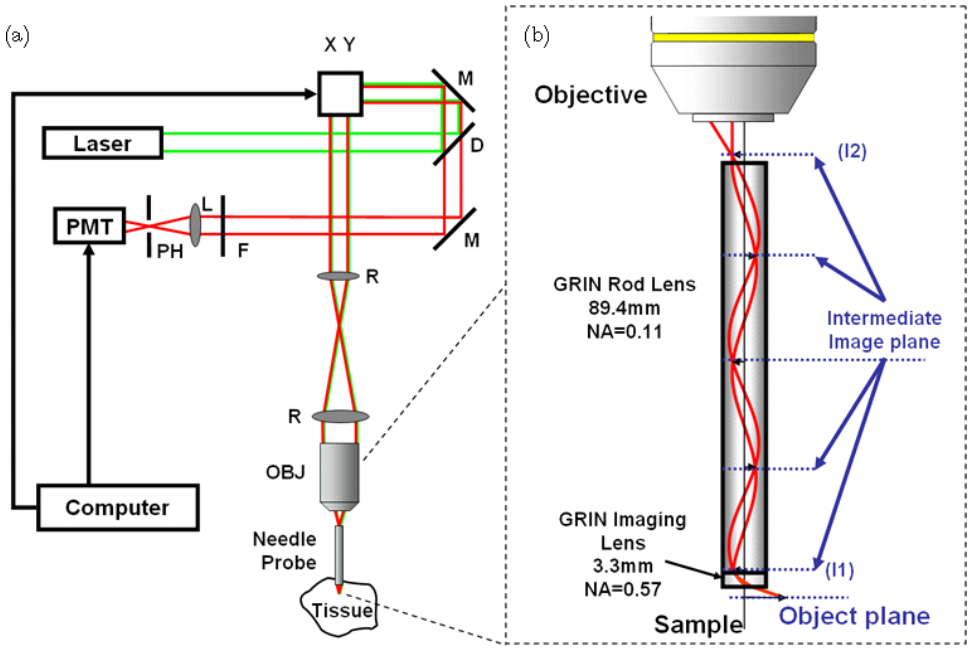

Fig. 1. (a) Schematics of the laser scanning fluorescence microscopy imaging system. M: mirror; D: dichroic mirror; R: relay lens; L: lens; OBJ: objective; PH: pin hole; PMT: Photomultiplier Tube; XY: XY scanner. (b) Schematics of the gradient-index (GRIN) lens based microendoscopy. Red light trace is simulated by ZEMAX.

directed into the emission filter by a dichroic mirror (D) which separated the excitation light from the fluorescence emission light. The fluorescence signal, after passing the emission filter and confocal pinhole, was detected by a photomultiplier tube (PMT). The excitation and filter wavelengths could be readily modified based on the excitation and emission properties of the fluorescence markers used in the study. In this study, we used human MDA-MB-231 breast tumor xenografts stably expressing tandem dimer (td)Tomato red fluorescent protein (RFP), which has the high fluorescence quantum yield of 0.69[54,55] (excitation wavelength: 532 nm, emission wavelength range: 580–660 nm), to test our imaging system. To generate an *en face* fluorescence image, the illumination point was raster-scanned by a resonance scanner and a galvanometer mirror to achieve a real-time speed of 8–10 Hz.

2.2. *Needle-based microendoscope*

The microendoscopy probe consists of a GRIN rod relay lens and a GRIN imaging lens (NSG America Inc., USA). The GRIN rod relay lens is 2-pitch long (89.4 mm) with a numerical aperture (NA) of 0.11, and the GRIN imaging lens is 3.3 mm long and has the high NA of 0.57. Overall, the needle probe is 1 mm in diameter and 92.7 mm in length. Figure 1(b) shows the diagram of the GRIN lens-based microendoscopy needle probe. The physics of GRIN lenses indicates that the plane at a distance d_1 away from the back of GRIN lenses and the conjugate imaging plane at a distance d_2 in front of GRIN lenses [see Fig. 2(a)] have the relation of[56]:

$$d_2 = \frac{(n_1 n_2/\sqrt{A})\sin(\sqrt{A}L) + n_2 n_0 \cos(\sqrt{A}L) d_1}{n_0^2\sqrt{A}\sin(\sqrt{A}L)d_1 - n_1 n_0 \cos(\sqrt{A}L)}, \tag{1}$$

where A is a wavelength-dependent constant for a particular lens, L is the length of the GRIN lens, and n_0, n_1, n_2 are the indices of refraction of GRIN lenses on axis, object space, and image space, respectively. The equation applies to both GRIN rod relay lens and GRIN imaging lens. GRIN rod relay lens is designed to relay images from one end to the other end. Therefore, the length L is typically chosen as multiple half-integer pitches such that $\sin(\sqrt{A}L) = 0$. On the other hand, the design of GRIN imaging lens is aimed to provide different working distances and magnifications while maintaining image quality such as high resolution and low field curvature. Therefore, depending on the design, parameters A and L will be different.

Based on our design, Eq. (1) simplifies to $d_2^r = -\frac{n_2}{n_1} d_1^r$ for the GRIN rod relay lens part. The minus sign is because the definition of orientations at both ends is opposite [see Fig. 2(a)]. In other words, the beam spot moves with the same distance and in the

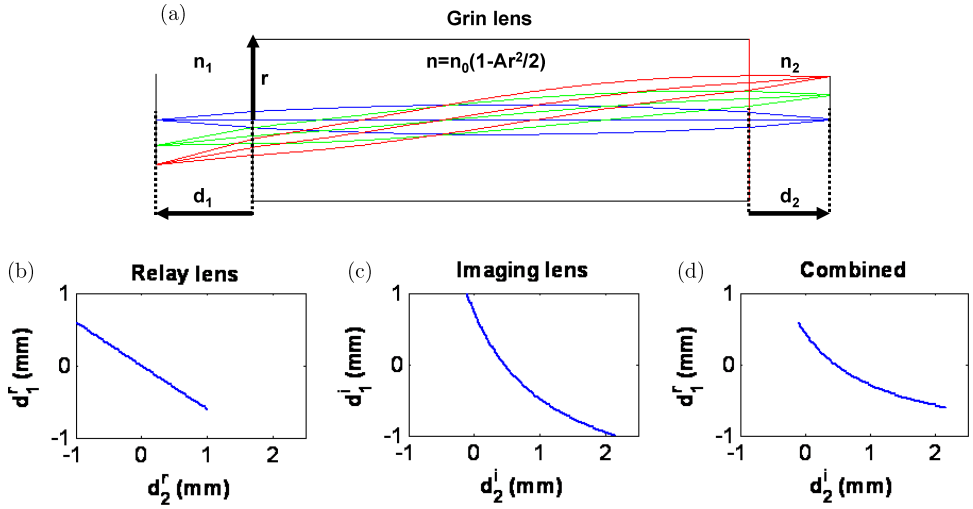

Fig. 2. (a) Diagram of image formation by a GRIN lens. Rays are traced by ZEMAX. (b)–(d) Relationship of d_1 and d_2 of the relay lens, imaging lens, and the cascade combination.

same direction as the entry site (focus tracking).[57] In our case, $n_1 = 1$ in air and $n_2 = 1.666$ on axis of GRIN imaging lens. For the GRIN imaging lens part, Eq. (1) specifies the relation between $d_1^i (= -d_2^r)$ and d_2^i by $n_0 = 1.666$, $n_1 = 1.610$, $n_2 = 1$, $\sqrt{A} = 0.786\,\text{mm}^{-1}$, and $L = 3.3\,\text{mm}$. As a result, by changing the entrance focus position d_1^r, the overall GRIN lens assembly working distance d_2^i can be changed accordingly within a certain range. Figures 2(b)–2(d) show the relationship for rod relay lens, imaging lens, and the combined GRIN lens assembly.

2.3. *tdTomato-expressing breast cancer cell line and breast cancer xenograft model*

A triple-negative human breast cancer cell line, MDA-MB-231, originally expanded from a pleural effusion, was obtained from the American Type Culture Collection. Plasmid DNA encoding tdTomato (pRSETB-tdTomato) was kindly donated by Professor Roger Tsien (University of California, San Diego),[54] cloned into the mammalian expression vector pEF-1α-myc/his (Invitrogen, Carlsbad, CA) generating pEF-1α-tdTomato.[55] pEF-1α-tdTomato was stably transfected into MDA-MB-231 cells using the Amaxa Nucleofector II instrument (Amaxa Biosystems, Gaithersburg, MD), followed by fluorescence-activated cell sorting (FACS) of tdTomato-fluorescing cells, and further expansion without antibiotics, which was performed by Winnard Jr. *et al.* as previously described.[55] Prior to inoculation, MDA-MB-231-tdTomato cells displayed intense tdTomato fluorescence in cell culture as tested with live cell fluorescence microscopy.[55]

One hundred thousand to two million MDA-MB-231-tdTomato cells were orthotopically inoculated in four sites of the mammary fat pad of anesthetized female athymic nude mice as previously described.[58] Tumor xenografts reached their final experimental size of about 5–150 mm^3 within 4–6 weeks. *In vivo* whole-body fluorescence imaging of MDA-MB-231-tdTomato tumor xenografts was performed using a commercially available optical imaging system, the Xenogen IVIS 200 Spectrum (Caliper Life Sciences, Hopkinton, MA) under isofluorane anesthesia. Following *in vivo* optical imaging, mice were sacrificed, and tumor xenografts were cut into 2 mm-thick fresh tumor slices throughout the tumor using an Acrylic Adjustable Tissue Slicer (12 mm D up to 25 mm W; Braintree Scientific, Inc., Braintree, MA), and Tissue Slicer Blades (Braintree Scientific). These breast tissue slices were fixed in formalin and used for *ex vivo* endomicroscopic imaging.

3. Results

3.1. *System calibration*

The system performance characteristics were first calibrated using a US air force resolution chart. The imaging field-of-view was measured by estimating the diameter of the circular imaging area. The transverse resolution was determined by fitting the one-dimensional intensity profile of the sharp edges

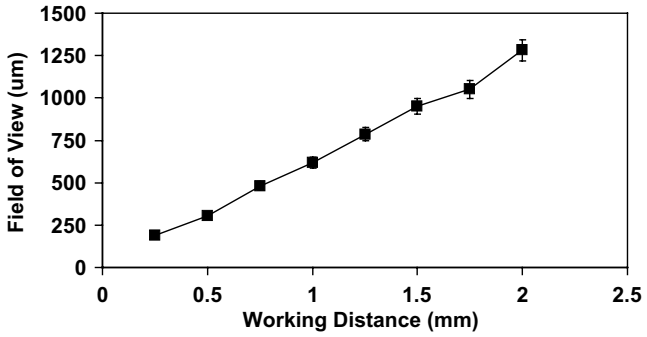

(a)

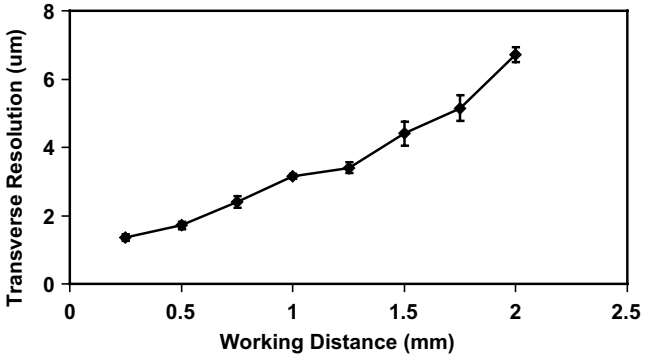

(b)

Fig. 3. (a) Plot of field-of-view (FOV) versus working distance. (b) Plot of transverse resolution versus working distance for the microendoscopic fluorescence molecular imaging.

of resolution charts with the sinc^2 function (edge spread function).

Figure 3 plots the FOV and transverse resolution versus the working distance. Figure 3(a) shows that the imaging FOV varied from ∼0.19 mm in diameter to ∼1.28 mm in diameter with the working distance from 0.25 mm to 2 mm. Figure 3(b) shows the transverse resolution changes from ∼1.3 to ∼6.7 μm correspondingly. The finest resolution measured (1.3 μm) was approximately three times larger than the theoretical diffraction limits of 0.57-NA optics (0.46 μm), which was possibly due to the spatial aberration of GRIN lenses.[52]

3.2. *In vivo fluorescence molecular imaging*

Figure 4 shows representative whole-body fluorescence images of MDA-MB-231-tdTomato tumor xenografts in the mammary fat pads of athymic nude mice measured with 535 nm excitation and 600 nm emission filters on the Xenogen IVIS 200 Spectrum. The photographic image in Fig. 4(a)

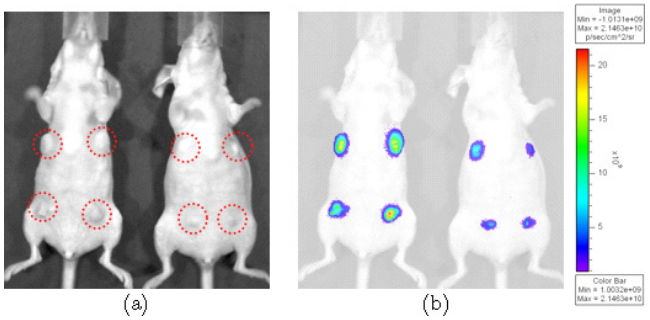

(a) (b)

Fig. 4. (a) Photographic image of mice with four MDA-MB-231-tdTomato tumors of slightly different sizes.

displays the nodules from MDA-MB-231-tdTomato tumors, which were circled with red dotted lines, growing in the mammary fat pad of these mice. Intense tdTomato fluorescence was detected in all MDA-MB-231-tdTomato tumor xenografts as shown in Fig. 4(b), and not in any other body part, resulting in high positive tumor fluorescence contrast. Such high contrast was optimal for testing our novel optical needle-based fluorescence molecular imaging device as described in the following.

3.3. *Ex vivo microendoscopic fluorescence molecular imaging*

Figure 5 shows the through-needle fluorescence microscopy of the excised human MDA-MB-231-tdTomato breast cancer xenograft constitutively expressing fluorescing tdTomato protein. Figures 5(a)–5(c) show abundant clusters of fluorescently labeled cancer cells, while Figs. 5(d)–5(f) show regions with sparse tumor cells. Note that single cells or cell clusters can be visualized. These results demonstrate that fluorescence molecular imaging with our 1 mm needle-imaging device is feasible in these *ex vivo* studies. In addition, it is evident from the images in Fig. 5 that at microscopic scale, the tumor is heterogeneous, while the macroscopic whole-body images shown in Fig. 4 detected a relatively homogeneous fluorescent signal from each tumor.

4. Perspectives on *In Vivo* Animal Imaging and Clinical Translations

Stereotactic core needle biopsy uses needles with 11–14 Gauge size (2.1–3.0 mm).[2,59–61] Optical methods, based on light, can be delivered through thin optical fibers and miniaturized micro-optics to be interfaced with standard biopsy devices for more

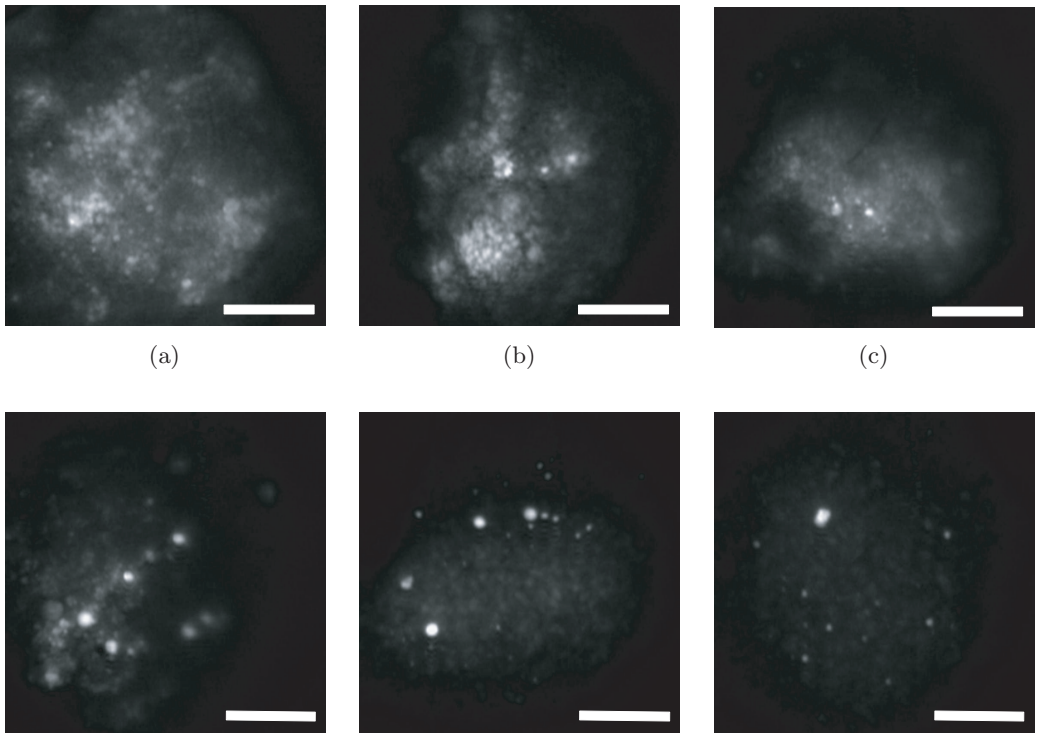

Fig. 5. Microendoscopic fluorescence molecular imaging in different tumor regions of a breast tumor xenograft model constitutively expressing human MDA-MB-231-tdTomato breast cancer cells grown in the mammary fat pad athymic nude mice. Bar: 200 μm.

accurate targeting of breast cancer. Previous studies have shown that different optical imaging and spectroscopy methods, such as OCT, confocal and multi-photon microscopy, and fluorescence imaging can be performed through either flexible endoscopes or needle imaging devices.[49,51–53,57,62–69] Reported needle-based devices for breast tissue characterization include low-coherence interferometry[20,32,33] and spectroscopy.[14,34–36] The needle-based fluorescence molecular imaging results presented here clearly demonstrate that getting an additional microscopic view of the breast cancer tissue in addition to detecting the same signal by whole-body imaging provides valuable additional information. The change in scale from macroscopic to microscopic opens up new possibilities for the evaluation of tumor heterogeneity and molecular events at the cellular or subcellular level. The heterogeneity detected in our microscopic images most likely originated from regions in which fluorescing MDA-MB-231-tdTomato cancer cells resided next to non-fluorescing portions of the tumor microenvironment, such as non-fluorescing stromal, vascular, and inflammatory cells, as well as the non-fluorescing extracellular tumor matrix.[70]

Such needle-based fluorescence imaging has a strong potential to further develop into a miniaturized imaging device to be integrated with standard core needle biopsy procedures to provide detailed tissue molecular information, *in vivo* and in real-time, before tissue removal. Figure 3 suggests that the FOV can reach 1–2 mm (or larger) depending on the working distance. A millimeter-level FOV is approaching the size of tissues sampled by biopsy needle. Therefore, this technology can provide a "first look" at tissue to be biopsied, thereby reducing the chance of missing cancers or unnecessary biopsies.

Figure 6 illustrates the integration of our needle imaging device with a biopsy needle for fluorescence molecular imaging, which we are proposing for use during breast biopsy procedures for microscopic guidance through the biopsy path in real time. This needle imaging device consists of one gradient-index (GRIN) rod lens and one GRIN imaging lens as described previously. A microprism is placed at the distal tip of the needle imaging device to perform side-view imaging with the aid of a standard core biopsy needle. The imaging FOV and resolution will be determined by the working distance. Such a

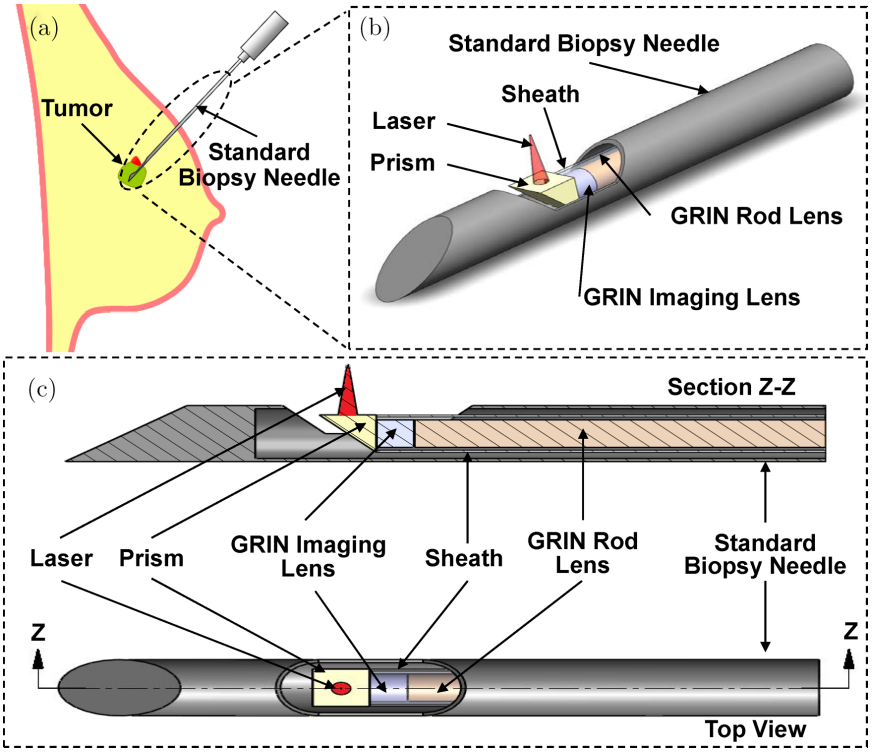

Fig. 6. (a) Interfacing of needle-based fluorescence molecular imaging device with standard core biopsy needle. (b) 3D solid view and (c) cross-sectional view of the needle imaging probe.

needle imaging device has a definite potential to be translated into clinical molecular imaging for breast cancer detection.

5. Conclusion

In summary, we have engineered and initially evaluated a needle-based microendoscopy device for fluorescence molecular imaging of breast cancer. The imaging FOV and resolution of this system can be varied with different working distance. Imaging of tdTomato red fluorescent protein (RFP) labeled tumor cells in a xenograft model of human MDA-MB-231-tdTomato breast cancer cells revealed clusters of fluorescently labeled cells in some tumor regions, and isolated, sporadic cells in other tumor regions, likely due to the heterogeneity of these breast tumors. This needle imaging microendoscopy holds strong potential to be translated into the clinic for real-time breast biopsy guidance.

Acknowledgments

We thank Jerry Wierwille (University of Maryland), Nicolas Bensaid (Institut d'Optique, France), and Hongzhou Ma (Thorlabs, Inc.) for technical assistances. This work was supported in part by the Nano-Biotechnology Award of the State of Maryland, the Minta Martin Foundation, the General Research Board (GRB) Award of the University of Maryland, and the University of Maryland Baltimore (UMB) and College Park (UMCP) Seed Grant Program, and the Prevent Cancer Foundation (to Y.C.). Support from NIH P50 CA103175 (JHU ICMIC Program, to V.R.) and NIH CA134695 (to K.G.) is gratefully acknowledged.

References

1. "Cancer Facts & Figures 2009," *American Cancer Society*, p. 4 (2009).
2. R. J. Jackman, K. W. Nowels, J. Rodriguez-Soto, F. A. Marzoni Jr., S. I. Finkelstein, M. J. Shepard, "Stereotactic, automated, large-core needle biopsy of nonpalpable breast lesions: False-negative and histologic underestimation rates after long-term follow-up," *Radiology* **210**, 799–805 (1999).
3. V. I. Shah, U. Raju, D. Chitale, V. Deshpande, N. Gregory, V. Strand, "False-negative core needle biopsies of the breast: An analysis of clinical, radiologic, and pathologic findings in 27 consecutive cases of missed breast cancer," *Cancer* **97**, 1824–1831 (2003).
4. M. J. Chare, C. I. Flowers, C. J. O'Brien, A. Dawson, "Image-guided core biopsy in patients

with breast disease," *Br. J. Surg.* **83**, 1415–1416 (1996).
5. H. I. Vargas, M. P. Vargas, K. D. Gonzalez, R. Venegas, M. Canet, M. Burla, K. Eldrageely, I. Khalkhali, "Diagnosis of palpable breast masses: Ultrasound-guided large core biopsy in a multidisciplinary setting," *Am. Surg.* **70**, 867–871 (2004).
6. J. Frayne, G. F. Sterrett, J. Harvey, P. Goodwin, J. Townsend, D. Ingram, R. W. Parsons, "Stereotactic 14 gauge core-biopsy of the breast: Results from 101 patients," *Aust. N. Z. J. Surg.* **66**, 585–591 (1996).
7. A. J. Evans, J. P. Whitlock, H. C. Burrell, S. E. Pinder, I. O. Ellis, J. G. Geraghty, A. H. Lee, A. R. Wilson, "A comparison of 14 and 12 gauge needles for core biopsy of suspicious mammographic calcification," *Br. J. Radiol.* **72**, 1152–1154 (1999).
8. B. W. Pogue, S. P. Poplack, T. O. McBride, W. A. Wells, K. S. Osterman, U. L. Osterberg, K. D. Paulsen, "Quantitative hemoglobin tomography with diffuse near-infrared spectroscopy: Pilot results in the breast," *Radiology* **218**, 261–266 (2001).
9. V. Ntziachristos, A. G. Yodh, M. Schnall, B. Chance, "Concurrent MRI and diffuse optical tomography of breast after indocyanine green enhancement," *Proc. Nat. Acad. Sci. U.S.A.* **97**, 2767–2772 (2000).
10. X. Intes, J. Ripoll, Y. Chen, S. Nioka, A. G. Yodh, B. Chance, "*In vivo* continuous-wave optical breast imaging enhanced with indocyanine green," *Med. Phys.* **30**, 1039–1047 (2003).
11. Q. Zhang, T. J. Brukilacchio, A. Li, J. J. Stott, T. Chaves, T. Wu, M. Chorlton, E. Rafferty, R. H. Moore, D. B. Kopans, D. A. Boas, "Coregistered tomographic X-ray and optical breast imaging: Initial results," *J. Biomed. Opt.* **10**, 024033 (2005).
12. R. Choe, S. D. Konecky, A. Corlu, K. Lee, T. Durduran, D. R. Busch, S. Pathak, B. J. Czerniecki *et al.*, "Differentiation of benign and malignant breast tumors by *in-vivo* three-dimensional parallel-plate diffuse optical tomography," *J. Biomed. Opt.* **14**, 024020 (2009).
13. B. J. Tromberg, N. Shah, R. Lanning, A. Cerussi, J. Espinoza, T. Pham, L. Svaasand, J. Butler, "Noninvasive *in vivo* characterization of breast tumors using photon migration spectroscopy," *Neoplasia* **2**, 26–40 (2000).
14. C. Zhu, E. Burnside, G. Sisney, L. Salkowski, J. Harter, B. Yu, N. Ramanujam, "Fluorescence spectroscopy: An adjunct diagnostic tool to image guided core needle biopsy of the breast," *IEEE Trans. Biomed. Eng.* (2009).
15. Z. Volynskaya, A. S. Haka, K. L. Bechtel, M. Fitzmaurice, R. Shenk, N. Wang, J. Nazemi, R. R. Dasari, M. S. Feld, "Diagnosing breast cancer using diffuse reflectance spectroscopy and intrinsic fluorescence spectroscopy," *J. Biomed. Opt.* **13**, 024012 (2008).
16. A. Alimova, A. Katz, V. Sriramoju, Y. Budansky, A. A. Bykov, R. Zeylikovich, R. R. Alfano, "Hybrid phosphorescence and fluorescence native spectroscopy for breast cancer detection," *J. Biomed. Opt.* **12**, 014004 (2007).
17. I. J. Bigio, S. G. Bown, G. Briggs, C. Kelley, S. Lakhani, D. Pickard, P. M. Ripley, I. G. Rose, C. Saunders, "Diagnosis of breast cancer using elastic-scattering spectroscopy: Preliminary clinical results," *J. Biomed. Opt.* **5**, 221–228 (2000).
18. S. A. Boppart, W. Luo, D. L. Marks, K. W. Singletary, "Optical coherence tomography: Feasibility for basic research and image-guided surgery of breast cancer," *Breast Cancer Res. Treat.* **84**, 85–97 (2004).
19. P. L. Hsiung, D. R. Phatak, Y. Chen, A. D. Aguirre, J. G. Fujimoto, J. L. Connolly, "Benign and malignant lesion in the human breast depicted with ultrahigh resolution and dimensional optical coherence tomography," *Radiology* **244**, 865–874 (2007).
20. B. D. Goldberg, N. V. Iftimia, J. E. Bressner, M. B. Pitman, E. Halpern, B. E. Bouma, G. J. Tearney, "Automated algorithm for differentiation of human breast tissue using low coherence interferometry for fine needle aspiration biopsy guidance," *J. Biomed. Opt.* **13**, 014014 (2008).
21. E. M. Sevick-Muraca, R. Sharma, J. C. Rasmussen, M. V. Marshall, J. A. Wendt, H. Q. Pham *et al.*, "Imaging of lymph flow in breast cancer patients after microdose administration of a near-infrared fluorophore: Feasibility study," *Radiology* **246**, 734–741 (2008).
22. C. Bremer, V. Ntziachristos, B. Weitkamp, G. Theilmeier, W. Heindel, R. Weissleder, "Optical imaging of spontaneous breast tumors using protease sensing 'smart' optical probes," *Invest. Radiol.* **40**, 321–327 (2005).
23. Y. Hama, Y. Koyama, Y. Urano, P. L. Choyke, H. Kobayashi, "Simultaneous two-color spectral fluorescence lymphangiography with near infrared quantum dots to map two lymphatic flows from the breast and the upper extremity," *Breast Cancer Res. Treat.* **103**, 23–28 (2007).
24. R. E. Lenkinski, M. Ahmed, A. Zaheer, J. V. Frangioni, S. N. Goldberg, "Near-infrared fluorescence imaging of microcalcification in an animal model of breast cancer," *Acad. Radiol.* **10**, 1159–1164 (2003).
25. C. Li, T. R. Greenwood, K. Glunde, "Glucosamine-bound near-infrared fluorescent probes with lysosomal specificity for breast tumor imaging," *Neoplasia* **10**, 389–398 (2008).
26. A. Parrish, E. Halama, M. T. Tilli, M. Freedman, P. A. Furth, "Reflectance confocal microscopy for characterization of mammary ductal structures and

development of neoplasia in genetically engineered mouse models of breast cancer," *J. Biomed. Opt.* **10**, 051602 (2005).
27. L. R. Bickford, G. Agollah, R. Drezek, T. K. Yu, "Silica-gold nanoshells as potential intraoperative molecular probes for HER2-overexpression in *ex vivo* breast tissue using near-infrared reflectance confocal microscopy," *Breast Cancer Res. Treat.* in press (2009).
28. D. K. Bird, L. Yan, K. M. Vrotsos, K. W. Eliceiri, E. M. Vaughan, P. J. Keely, J. G. White, N. Ramanujam, "Metabolic mapping of MCF10A human breast cells via multiphoton fluorescence lifetime imaging of the coenzyme NADH," *Cancer Res.* **65**, 8766–8773 (2005).
29. M. W. Conklin, P. P. Provenzano, K. W. Eliceiri, R. Sullivan, P. J. Keely, "Fluorescence lifetime imaging of endogenous fluorophores in histopathology sections reveals differences between normal and tumor epithelium in carcinoma *in situ* of the breast," *Cell Biochem. Biophys.* **53**, 145–157 (2009).
30. M. T. Tilli, M. C. Cabrera, A. R. Parrish, K. M. Torre, M. K. Sidawy, A. L. Gallagher, E. Makariou, S. A. Polin, M. C. Liu, P. A. Furth, "Real-time imaging and characterization of human breast tissue by reflectance confocal microscopy," *J. Biomed. Opt.* **12**, 051901 (2007).
31. C. Zeng, S. Vangveravong, J. Xu, K. C. Chang, R. S. Hotchkiss, K. T. Wheeler, D. Shen, Z. P. Zhuang, H. F. Kung, R. H. Mach, "Subcellular localization of sigma-2 receptors in breast cancer cells using two-photon and confocal microscopy," *Cancer Res.* **67**, 6708–6716 (2007).
32. A. M. Zysk, S. G. Adie, J. J. Armstrong, M. S. Leigh, A. Paduch, D. D. Sampson, F. T. Nguyen, S. A. Boppart, "Needle-based refractive index measurement using low-coherence interferometry," *Opt. Lett.* **32**, 385–387 (2007).
33. N. V. Iftimia, B. E. Bouma, M. B. Pitman, B. Goldberg, J. Bressner, G. J. Tearney, "A portable, low coherence interferometry based instrument for fine needle aspiration biopsy guidance," *Rev. Sci. Instrum.* **76**, 064301 (2005).
34. R. Manoharan, K. Shafer, L. Perelman, J. Wu, K. Chen, G. Deinum, M. Fitzmaurice, J. Myles, J. Crowe, R. R. Dasari, M. S. Feld, "Raman spectroscopy and fluorescence photon migration for breast cancer diagnosis and imaging," *Photochem. Photobiol.* **67**, 15–22 (1998).
35. C. Lubawy, N. Ramanujam, "Endoscopically compatible near-infrared photon migration probe," *Opt. Lett.* **29**, 2022–2024 (2004).
36. B. Yu, E. S. Burnside, G. A. Sisney, J. M. Harter, C. Zhu, A. H. Dhalla, N. Ramanujam, "Feasibility of near-infrared diffuse optical spectroscopy on patients undergoing image guided core-needle biopsy," *Opt. Express* **15**, 7335–7350 (2007).
37. R. Weissleder, "Molecular imaging in cancer," *Science* **312**, 1168–1171 (2006).
38. D. Piwnica-Worms, D. P. Schuster, J. R. Garbow, "Molecular imaging of host-pathogen interactions in intact small animals," *Cell. Microbiol.* **6**, 319–331 (2004).
39. T. F. Massoud, S. S. Gambhir, "Molecular imaging in living subjects: Seeing fundamental biological processes in a new light," *Genes Dev.* **17**, 545–580 (2003).
40. R. G. Blasberg, "Molecular imaging and cancer," *Mol. Cancer Ther.* **2**, 335–343 (2003).
41. J. F. Lovell, G. Zheng, "Activatable smart probes for molecular optical imaging and therapy," *J. Innov. Opt. Health Sci.* **1**, 45–61 (2008).
42. S. Achilefu, "Lighting up tumors with receptor-specific optical molecular probes," *Technol. Cancer Res. Treat.* **3**, 393–409 (2004).
43. R. Weissleder, M. J. Pittet, "Imaging in the era of molecular oncology," *Nature* **452**, 580–589 (2008).
44. C. Bremer, C. H. Tung, A. Bogdanov, Jr., R. Weissleder, "Imaging of differential protease expression in breast cancers for detection of aggressive tumor phenotypes," *Radiology* **222**, 814–848 (2002).
45. R. Weissleder, C. H. Tung, U. Mahmood, A. Bogdanov, "*In vivo* imaging of tumors with protease-activated near-infrared fluorescent probes," *Nat. Biotech.* **17**, 375–378 (1999).
46. S. Achilefu, R. B. Dorshow, J. E. Bugaj, R. Rajagopalan, "Novel receptor-targeted fluorescent contrast agents for *in vivo* tumor imaging," *Invest. Radiol.* **35**, 479–485 (2000).
47. Y. Chen, C. P. Mu, X. Intes, D. Blessington, B. Chance, "Near-infrared phase cancellation instrument for fast and accurate localization of fluorescent heterogeneity," *Rev. Sci. Instrum.* **74**, 3466–3473 (2003).
48. V. Ntziachristos, C. H. Tung, C. Bremer, R. Weissleder, "Fluorescence molecular tomography resolves protease activity *in vivo*," *Nat. Med.* **8**, 757–760 (2002).
49. B. A. Flusberg, E. D. Cocker, W. Piyawattanametha, J. C. Jung, E. L. M. Cheung, M. J. Schnitzer, "Fiber-optic fluorescence imaging," *Nat. Methods* **2**, 941–950 (2005).
50. H. Wang, T. B. Huff, Y. Fu, K. Y. Jia, J. X. Cheng, "Increasing the imaging depth of coherent anti-Stokes Raman scattering microscopy with a miniature microscope objective," *Opt. Lett.* **32**, 2212–2214 (2007).
51. J. C. Jung, M. J. Schnitzer, "Multiphoton endoscopy," *Opt. Lett.* **28**, 902–904 (2003).

52. P. Kim, M. Puoris'haag, D. Cote, C. P. Lin, S. H. Yun, "*In vivo* confocal and multiphoton microendoscopy," *J. Biomed. Opt.* **13**, 010501 (2008).
53. M. J. Levene, D. A. Dombeck, K. A. Kasischke, R. P. Molloy, W. W. Webb, "*In vivo* multiphoton microscopy of deep brain tissue," *J. Neurophysiol.* **91**, 1908–1912 (2004).
54. N. C. Shaner, R. E. Campbell, P. A. Steinbach, B. N. Giepmans, A. E. Palmer, R. Y. Tsien, "Improved monomeric red, orange and yellow fluorescent proteins derived from Discosoma sp. red fluorescent protein," *Nat. Biotechnol.* **22**, 1567–1572 (2004).
55. P. T. Winnard, Jr., J. B. Kluth, V. Raman, "Noninvasive optical tracking of red fluorescent protein-expressing cancer cells in a model of metastatic breast cancer," *Neoplasia* **8**, 796–806 (2006).
56. F. C. McNeillie, J. Thomson, I. S. Ruddock, "The imaging properties of gradient index optical fibres," *Eur. J. Phys.* **25**, 479–487 (2004).
57. T. Q. Xie, S. G. Guo, Z. P. Chen, D. Mukai, M. Brenner, "GRIN lens rod based probe for endoscopic spectral domain optical coherence tomography with fast dynamic focus tracking," *Opt. Express* **14**, 3238–3246 (2006).
58. K. Glunde, C. A. Foss, T. Takagi, F. Wildes, Z. M. Bhujwalla, "Synthesis of 6′-O-lissamine-rhodamine B-glucosamine as a novel probe for fluorescence imaging of lysosomes in breast tumors," *Bioconjug. Chem.* **16**, 843–851 (2005).
59. S. H. Parker, J. D. Lovin, W. E. Jobe, B. J. Burke, K. D. Hopper, W. F. Yakes, "Nonpalpable breast lesions: Stereotactic automated large-core biopsies," *Radiology* **180**, 403–407 (1991).
60. S. H. Parker, J. D. Lovin, W. E. Jobe, J. M. Luethke, K. D. Hopper, W. F. Yakes, B. J. Burke, "Stereotactic breast biopsy with a biopsy gun," *Radiology* **176**, 741–747 (1990).
61. L. E. Philpotts, N. A. Shaheen, D. Carter, R. C. Lange, C. H. Lee, "Comparison of rebiopsy rates after stereotactic core needle biopsy of the breast with 11-gauge vacuum suction probe versus 14-gauge needle and automatic gun," *Am. J. Roentgenol.* **172**, 683–687 (1999).
62. A. F. Gmitro, D. Aziz, "Confocal microscopy through a fiber-optic imaging bundle," *Opt. Lett.* **18**, 565–567 (1993).
63. K. Carlson, M. Chidley, K. B. Sung, M. Descour, A. Gillenwater, M. Follen, R. Richards-Kortum, "*In vivo* fiber-optic confocal reflectance microscope with an injection-molded plastic miniature objective lens," *Appl. Opt.* **44**, 1792–1797 (2005).
64. C. Liang, K. B. Sung, R. R. Richards-Kortum, M. R. Descour, "Design of a high-numerical-aperture miniature microscope objective for an endoscopic fiber confocal reflectance microscope," *Appl. Opt.* **41**, 4603–4610 (2002).
65. T. Xie, D. Mukai, S. Guo, M. Brenner, Z. Chen, "Fiber-optic-bundle-based optical coherence tomography," *Opt. Lett.* **30**, 1803–1805 (2005).
66. S. A. Boppart, B. E. Bouma, C. Pitris, G. J. Tearney, J. G. Fujimoto, M. E. Brezinski, "Forward-imaging instruments for optical coherence tomography," *Opt. Lett.* **22**, 1618–1620 (1997).
67. X. Li, C. Chudoba, T. Ko, C. Pitris, J. G. Fujimoto, "Imaging needle for optical coherence tomography," *Opt. Lett.* **25**, 1520–1522 (2000).
68. S. Han, M. V. Sarunic, J. Wu, M. Humayun, C. Yang, "Handheld forward-imaging needle endoscope for ophthalmic optical coherence tomography inspection," *J. Biomed. Opt.* **13**, 020505 (2008).
69. U. Utzinger, R. R. Richards-Kortum, "Fiber optic probes for biomedical optical spectroscopy," *J. Biomed. Opt.* **8**, 121–147 (2003).
70. K. Glunde, A. P. Pathak, Z. M. Bhujwalla, "Molecular-functional imaging of cancer: To image and imagine," *Trends Mol. Med.* **13**, 287–297 (2007).